https://doi.org/10.5194/egusphere-2023-2494
Preprint. Discussion started: 1 December 2023

Dakar Niño variability under global warming investigated by a high-resolution regionally coupled model

Shunya Koseki[1], Rúben Vázquez[2,3], William Cabos[2], Claudia Gutiérrez[2], Dmitry V. Sein[4,5] Marie-Lou Bachèlery[1]

[1]Geophysical Institute, University of Bergen / Bjerknes Centre for Climate Research, Bergen, 5007, Norway
[2]Departamento de Física y Matemátics, Universidad de Alcalá, Alcalá de Henares, 28805, Spain
[3]Instituto Universitario de Investigación Marina (INMAR), Universidad de Cádiz, Cádiz, 11510, Spain
[4]Alfred-Wegener Institute for Polar and Marine Research, Bremerhaven, 27570, Germany
[5]Shirshov Institute of Oceanography, Russian Academy of Science, Moscow, 117218, Russia

Correspondence to: Shunya Koseki (Shunya.Koseki@uib.no)

Abstract. In this study, we investigated the interannual variability of sea surface temperature (SST) along the northwest African coast and the strong Dakar Niño and Niña events, and their potential changes under the highest emission scenario RCP8.5 of global warming using a high-resolution regional coupled model. Our model accurately reproduces the SST seasonal cycle along the northwest African coast and its interannual variability in terms of amplitude, timing, and position of the maximum variability. Comparing the Dakar Niño variability between the 1980-2010 and 2069-2099 periods, we found that its variability intensifies under a warmer climate without changing its location and timing. The intensification is more pronounced during the Dakar Niñas (cold SST events) than during Niños (warm SST events) and the ocean temperature variability is connected more deeply with the Dakar Niño variability (vertical motion is more deeply correlated with Dakar Niño variability). The increase of Dakar Niño variability can be explained by the larger variability in meridional wind stresses, which is likely to be amplified in the future by enhanced land-sea thermal contrast and associated sea-level pressure anomalies elongated from the Iberian-Mediterranean area. In addition, the ocean temperature is warmed more effectively above 40m depth, where the temperature anomaly is maximum, i.e., the stratification is reinforced around 40m depth. This enhanced stratification may also lead to an increase in the amplitude of the Dakar Niño/Niña events.

1 Introduction

From a climatological aspect, the Senegal-Mauritania Frontal Zone (SMFZ, around 9°N-14°N and 20°W-16°W) is one of the most pronounced oceanic frontal zones generated along the eastern boundary current system. Here the cold waters of southward Canary Current and upwelling system (e.g., Barton et al., 1998; Perez-Hernandez et al., 2013; Vazquez et al., 2022) meet relatively warm tropical waters resulting in a steep sea surface temperature (SST) gradient (e.g., (Koseki et al., 2019; Ndoye et al., 2014; Sylla et al., 2019). The northern end of the SMFZ is around 19°N where the Canary Current joints with the north equatorial Current (e.g., Santana-Falcon et al., 2020) around Cape Blanc (e.g., Pastor et al., 2008). The Canary upwelling system is tightly connected with the equatorward alongshore wind associated with the Azores anti-cyclone (e.g.,

https://doi.org/10.5194/egusphere-2023-2494
Preprint. Discussion started: 1 December 2023

Davis et al., 1997) and highly dependent on the latitudinal migration of the Intertropical Convergence Zone (ITCZ, Sylla et al., 2019). Related to the enriched nutrients from the ocean subsurface, the SMFZ and Canary upwelling region also exhibit an active marine ecosystem (e.g., Aristegui et al., 2009; Gomez-Letona et al., 2017) and consequently, play an important role in local and regional fisheries such as sardinella from the northwestern Africa to the Iberian coasts in the north tropical-to-subtropical Atlantic (e.g., (Arrasate-Lopez et al., 2012; Becognee et al., 2006; Ndoye et al., 2014).

Apart from these climatological mean-state features, the SMFZ shows intense interannual variability in SST, so-called Dakar Niño (e.g., Oettli et al., 2016). Principally, Dakar Niño is driven by the local wind anomaly and it peaks between March and April according to Oettli et al. (2016). A similar mode of SST variability is found in the southeastern tropical Atlantic, which is Benguela Niño (e.g., Bachelery et al., 2020; Koungue et al., 2021; Koungue et al., 2019; Rouault et al., 2018). There, the interannual variability is not only by local wind fluctuations, but is also strongly linked to western equatorial winds that trigger the propagation of equatorial Kelvin waves and costal trapped waves off the African coast. The dominant contribution of equatorial dynamics to the southeastern Atlantic results in stronger Benguela Niño events compared to Dakar Niño events. In spite of that, the inter-annual SST variability in the Dakar system has a major influence on marine ecosystems. For instance, Lopez-Parages et al. (2020) showed that the distribution of round sardinella tends to be modified following the Dakar-Niño-like pattern initialized by El Niño variability in the tropical Pacific.

For sustainable development, including the fisheries sector, the understanding of climate variability under global warming draws more attention not only from the scientific community, but also from societies, stakeholders, and governments. Climate projections from Earth System Model (ESM), such as the Coupled Model Intercomparison Project Phase6 (CMIP6, Eyring et al., 2016), are one of the most common tools to investigate future climate change. These ESMs are state-of-the-art models that have been improved in many aspects for the simulation of the climate system and their use for climate prediction (e.g., Bracegirdle et al., 2020; Choudhury et al., 2022; Priestley et al., 2020). In contrast, model biases in the tropical Atlantic climate are a long-standing issue until CMIP6 and are very common in most of state-of-the-art ESMs (e.g., Cabos et al., 2017; Richter and Tokinaga, 2020; Richter and Xie, 2008; Voldoire et al., 2019). These biases are one of the main sources of uncertainty in climate projections and therefore, there is a necessity to utilize less systematically-biased ESMs to assess more plausible climate projections. Partially because of model errors mentioned above and relatively recent discovery of Dakar Niño (the first paper on this topic is Oettli et al. 2016), there are few studies on how the Dakar Niño variability would evolve under global warming while surveys on the equatorial Atlantic variability have been reported timely (e.g., Crespo et al., 2022; Yang et al., 2022).

There are several methodologies to alleviate model errors that have been proposed in the previous studies including the implementation of better parameterization (e.g., Deppenmeier et al., 2020), heat and/or momentum flux correction/anomaly coupling (e.g., Dippe et al., 2018; Toniazzo and Koseki, 2018; Voldoire et al., 2019), and interactive model ensembles (e.g., Shen et al., 2016); Counillon et al., 2023; Schevenhoven et al., 2023). Apart from these methodologies, resolution refinement is also beneficial to improve the model performance in the tropical Atlantic (e.g., de la Vara et al., 2020). Sylla et al. (2022), by assessing the archives of High Resoliution Model Intercomparison Project (HighResMIP, Haarsma et al., 2016), stressed

https://doi.org/10.5194/egusphere-2023-2494
Preprint. Discussion started: 1 December 2023

the limited benefits of model refinement to improve the Canary Current upwelling system. On the other hand, Vazquez et al. (2022) suggest that a high-resolution (mesoscale eddy-permitting scale) regional coupled model is able to represent the Canary Current upwelling systems and surface wind field.

This study, therefore, aims to unveil how the Dakar Niño variability would change in the future climate by adapting the reliable high-resolution regional coupled model used in Vazquez et al. (2022). This paper is structured as follows: Section 2 gives details on the regional coupled model, the experimental setup, and the reanalysis data. We will describe results of model simulations with brief evaluation comparing with reanalysis data in Section 3. Finally, we will give discussions on the results and summary of this study.

2 High-resolution regional coupled model

The regionally-coupled model ROM (e.g., Sein et al., 2020; Sein et al., 2015) configurations used in this study is the same as in Vazquez et al. (2022). It consists of a regional atmospheric component, limited-area Regional Model (REMO, e.g., Jacob, 2001) and global oceanic component, Max-Planck Institute Ocean Model (MPIOM, e.g., Jungclaus et al., 2013; Marsland et al., 2003). REMO has 25km horizontal resolution with 27 hybrid vertical levels. MPIOM adapts an orthogonal curvilinear horizontal grid system with shifted poles allowing to refine the focused region while a global domain can be maintained (for more details, see Sein et al., 2015). In our setting, MPIOM has 5 to 10km of horizontal resolution around the Iberian Peninsula and Cape Ghir at 31°N and 10°W upscaling gradually toward 100km in the Southern Ocean. The ROM's configuration domain utilized in this study is given in Fig.1. Air-sea coupling is active between REMO and MPIOM within the red rectangular shown in Fig.1. Outside of the active regional coupling, the MPIOM is forced by prescribed atmospheric forcing. The REMO is laterally forced by those prescribed atmospheric forcing.

In this study, ROM is integrated from 1950 to 2099 under historical and the Representative Concentration Pathway 8.5 (RCP8.5) forcing. The global atmospheric forcing is derived from the low-resolution Max Planck Institute ESM (MPI-ESM-LR, (Block and Mauritsen, 2013; Giorgetta et al., 2013). At detailed evaluation of the ROM configurations for 1950-2005 historical period with respect to observational products and forced by ERA-Interim (Dee et al., 2011) is demonstrated intensively by Cabos et al. (2020), Cabos et al. (2017), and Vazquez et al. (2022). Here, we analyze the data from 1980 to 2010 as present climate conditions and from 2069 to 2099 as future climate change referring to ROM_P and ROM_F, hereafter. For a brief evaluation of the ROM simulation, atmosphere and ocean reanalysis data provided by the European Centre for Medium Range Weather Forecast ERA5 (Hersbach et al., 2020) and ORAS5 (Zuo et al., 2019), during 1980-2010 and the satellite data of European Space Agency (ESA) SST Climate Change Initiative (CCI) product (Good, 2019) during 1981-2010 is used.

https://doi.org/10.5194/egusphere-2023-2494
Preprint. Discussion started: 1 December 2023

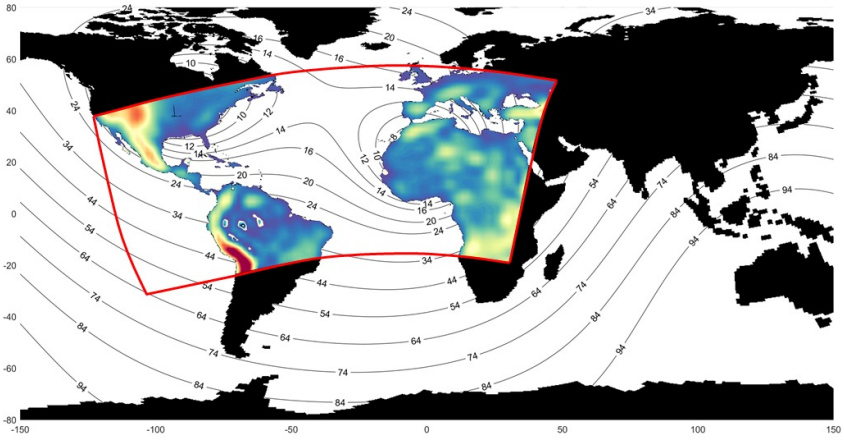

Figure 1: The schematic of the ROM's domain used in this study. REMO is the red-squared domain. The numbers denote the resolution of MPI-OM.

3. Results

3.1 Climatology and interannual variability

First, we assess the SMFZ seasonal cycle and its interannual variability as shown in Fig.2. The results show a clear seasonal cycle displacement of the SMFZ with the cold water penetrating more southward from February to April and being pushed more northward from August to October (Fig. 2a-d). This seasonal meridional migration of SST front could be associated with the seasonal cycle of the Canary Current and upwelling locational changes (Cropper et al., 2014; Pardo et al., 2011; Sylla et al., 2019) by displacing the surface water masses meridionally. Additionally, during winter to early spring, the Mauritania Current flows down to 14°N. Inversely, associated with the relaxation of the trade winds (e.g., Lazaro et al., 2005), the Mauritania Current reaches the Cape Blanc (around 20°N) associated with the cessation of upwelling south of this latitude (Mittelstaedt, 1991). The steep SST gradient is consistent with the SST seasonal cycle and locates at 10°N-12°N in February to April and 20°N-22°N in August to October. Coinciding with the position of the front, enhanced interannual variability appears in November and persists till May with a maximum peak of 1.2 K at 10°N-12°N between February and April (Fig. 2e). This period coincides with the preferred season of Dakar Niño/Niña (Oettli et al., 2016). Another moderate peak of variability is found from August to October at 20°N-22°N when the SST gradient reaches its second maximum. Similar to these patters of the SMFZ and Dakar Niño, the Angola-Benguela Frontal Zone (ABFZ, e.g, Colberg and Reason, 2006; Koseki et al., 2019) and Benguela Niño variability is maximized between February to April (e.g., Aristegui et al., 2009; Bachelery et al., 2020; Koseki and Koungue, 2021; Koungue et al., 2021; Koungue et al., 2019; Rouault et al., 2018). However, there are dissimilarities between the two coastal interannual modes: the SMFZ seasonal displacement is much wider than the ABFZ whose position is almost seasonally fixed (e.g., Koseki et al., 2019) and the Benguela Niño/Niña has more larger intensity than Dakar Niño/Niña because of the strong remote influence from the equator via equatorial and coastal Kelvin waves (e.g., Bachèlery et al., 2020; Koungue et al., 2019). The ESA SST shows a similar pattern of seasonality of SST, variability and SST gradient (Figs. 2b and f). Compared to the ERA5, the ESA SST is cooler in all months. This could be due to relatively-poor

https://doi.org/10.5194/egusphere-2023-2494
Preprint. Discussion started: 1 December 2023

representation of coastal upwelling in the ERA5 and ERA5 has a warm (Vazquez et al., 2022) bias. Conversely, the SST meridional gradient is much steeper in the ESA than the ERA5 maybe because the ESA has a finer resolution (0.05 degree) than the ERA5 (0.25 degree).

The ROMP simulation can reproduce the SMFZ well as shown in Figs. 2c compared with Fig 2a. At the lower latitude (EQ to 12°N), ROMP has cold SST biases in a whole year with respect to the ERA5 and ESA. Such cold SST bias can be seen at the higher latitude (18°N to 30°N), but they are moderate (Fig. 2b). According to Vazquez et al. (2023), coupling and higher-resolution SST allow a better representation of the North African Coastal Low Level Jet (e.g., Soares et al., 2019), which is a key pattern of the surface wind field along the North African coast. This good representation of the SMFZ is due to the finer resolution to permit meso-scale eddy and filaments in our focusing region in contrast to the common Earth system models like CMIP5 (Vazquez et al., 2022). The SST variability is also realistically represented in ROMP (Fig. 2g). The variability is maximized during March to April, which is slightly delayed from the observation. However, its amplitude is as strong as the ERA5 and weaker than ESA (Figs. 2e, f and g). The secondary peak during August to October can be well-captured.

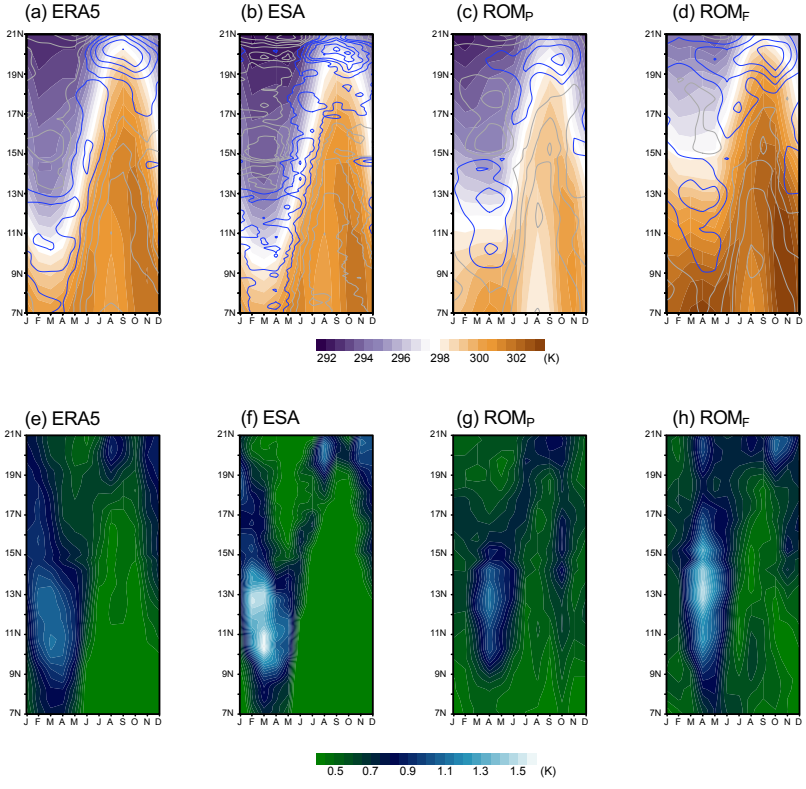

Figure 2: Hovmöller plot of (top) sea surface temperature (SST, color) and aboslute value of merdional SST gradient (K/100km, contour, interval is 0.2K/100km). The merdional SST gradient more than 0.5K/100km is shown by blue. Data are averaged between 21°W and 16°W for ERA5, ESA, ROMP and ROMF, respectively. (bottom) Same as top panels, but for the standard devitation of detrended SST. Unit is in Kelvin.

https://doi.org/10.5194/egusphere-2023-2494
Preprint. Discussion started: 1 December 2023

Under the highest emission scenario, this region experiences warming; the lower latitude is warmed up by 3 degree and higher latitude is by 1 degree (Fig. 2d). However, the SMFZ location is almost identically between ROM_P and ROM_F (not shown). Interestingly, the Dakar Niño variability is strengthened in both peaks in ROM_F while its timing does not change (Fig. 2h). This response of the Dakar Niño variability is opposite to that of the equatorial Atlantic variability reported recently (e.g., Crespo et al., 2022; Yang et al., 2022). The possible mechanism of this reinforcement will be given in the next subsection. Henceforth, we will focus on the month of March when the Dakar Niño variability is largest. Between present and future climate, the SST gradient in the frontal zone does not change its intensity and location simulated by the ROM (Figs. 2c and d).

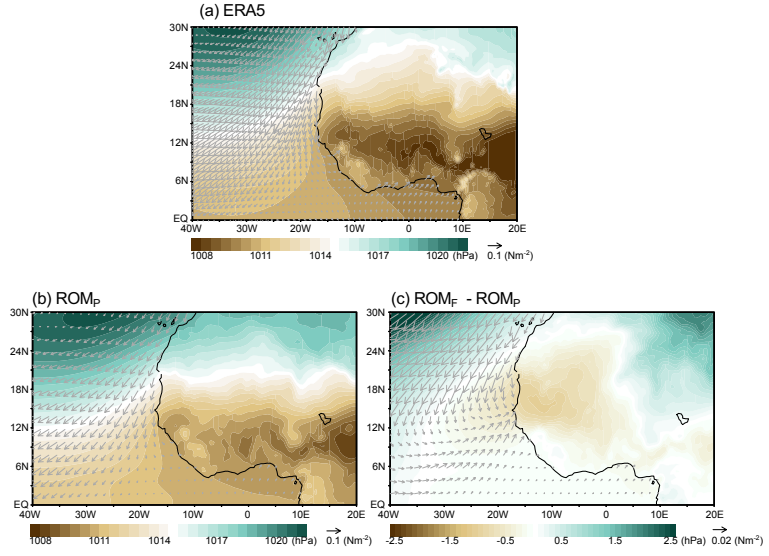

Figure 3: March-climatological sea level pressure (SLP in hPa, color) and wind stress (arrows) in (a) ERA5 and (b) ROM_P. (c) The difference in SLP and wind streess climatology in March between ROM_F and ROM_P.

As shown in Fig. S1, associated with the intense upwelling, the thermocline (20°C of temperature) tilts zonally (shallower in the east) in the observation (Fig. S1a). ROM_P can represent this zonal tilting of thermocline well and the steep vertical gradient is found around 40-60m depth along the coast (Fig. S1b). Under global warming, the thermocline tends to be deeper while the coastal vertical gradient seems stronger than that in ROM_P between 40 and 60m depth (Fig.S1b and c).

In March, the western Africa is covered by low pressure between 6°N and 15°N and the strong southerly wind blows along the western African coast (Fig. 3a). ROM_P simulates this atmospheric circulation realistically while the low pressure over the Sahel is slightly underestimated (Fig. 3b). As shown in Fig. 3c, the continental low pressure is partially deepened, especially, near the coastal area (10°N-24°N and 15°E to 0°E) where the surface temperature at 2m is intensively warmed by 5 degrees in ROM_F (not shown). This strong terrestrial warming can be explained by the desert amplification (e.g., Cook and Vizy, 2015; Zhou, 2016). Corresponding to this deepened low pressure, a cyclonic circulation anomaly is detected around 15°N and 15°W in Fig. 3c. This anomaly pattern is similar to climate projections by CMIP5 (Sylla et al., 2019). While the

https://doi.org/10.5194/egusphere-2023-2494
Preprint. Discussion started: 1 December 2023

upwelling-favorable wind intensifies at higher latitudes (18°N-30°N), onshore wind anomaly forms at lower latitude (12°N-15°N).

3.2 Dakar Niño variability

In this subsection, more details of the Dakar Niño modification under the highest emission scenario are investigated employing lag-correlation and composite analyses. These analyses are based on the Dakar Index in March defined as detrended interannual SST anomalies averaged over the 9°N-14°N/21°W-17°W box (Oettli et al., 2016).

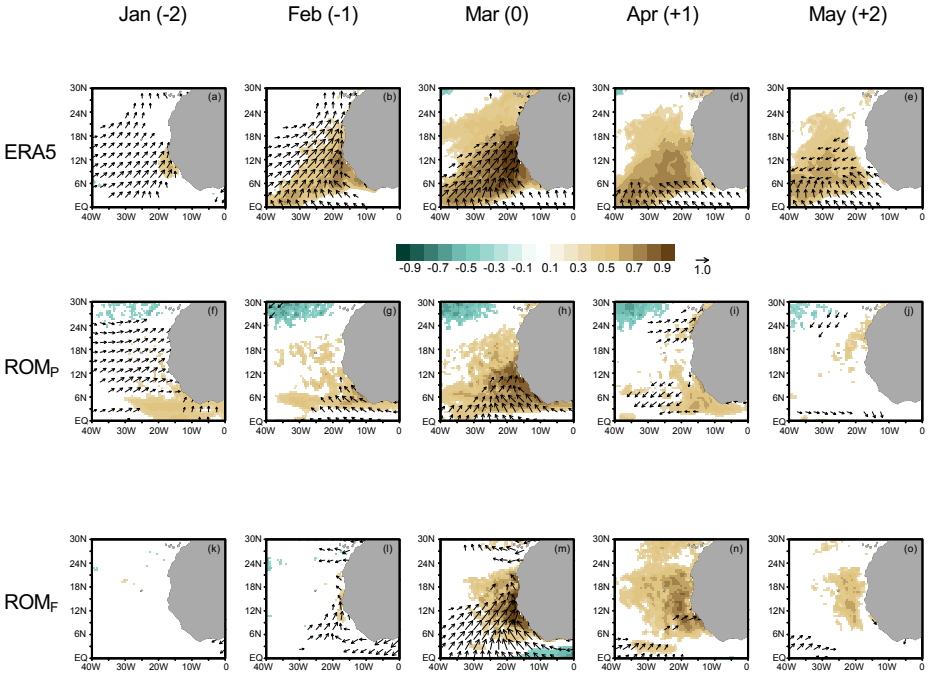

Figure 4: Lag-correlation plots between March Dakar Index (SST over 9°N-14°N and 21°W-17°W) and wind stress (vector) and SST (color). Only the correlation is shown satisfying $p < 0.05$ for (top) ERA5, (middle) ROM_P, and (bottom) ROM_F, respectively. From the left to the right, the panels show the lag-correlation from Janurary (-2) to May (+2).

In ERA5, positive surface wind correlation (southwesterly) and SST positive correlation are found along the west African coast in January, two months before the peak in March (Fig. 4a). The positive correlation becomes more intense in February to March (Figs.4a and c). In March, the significant correlation of surface wind is relatively localized below 15°N. After the peak of Dakar Niños, the surface wind correlation is more dominant only around the equator and offshore in April to May (Figs. 4d and e). The positive SST correlation seems to propagate westward, in particular around 6°N to 10°N, in April to May (Figs. 4d and e) and this might be related to Rossby wave propagation inducing the equatorial Atlantic Zonal mode in summer (e.g., Martin-Rey and Lazar, 2019). In ROM_P, the life-cycle of Dakar Niño variability is somewhat simulated well:

https://doi.org/10.5194/egusphere-2023-2494
Preprint. Discussion started: 1 December 2023

the surface wind correlated positively in January (Fig. 4f). Positive SST grows from January to March while the surface wind in February is not well simulated (Figs. 4f-h). The surface wind in March is more locally correlated as the ERA5 (Figs. 4c and h). After the peak, the positive SST correlation decays, but seems not to propagate westward clearly. However, a signal of westward propagation can be detected at 41m depth (around 6°N) in ROM_P (Fig. S1). Although the evolution of the ROM_F-simulated Dakar Niño and correlated surface wind in January and February are not as clear as ROM_P (Figs. 4k and l), the surface wind is correlated more broadly along the coast during March up to 18°N (Fig. 4m) while it is limited to 12°N in ROM_P (Fig. 4h). After the peak, the positive SST correlation moves westward more clearly like ERA5 even though its phase speed is slower than the ERA5 (Figs. 4n and o).

In ROM_P, the significant positive correlation concentrates between the surface and 40m depth and decreases to 100m depth, which is about 0.4 (Fig. 5a). In contrast, the ocean temperature correlates significantly with the Dakar Index more deeply down to 160m depth with 0.5 of correlation in ROM_F (Fig. 5c). This deeper connection of ocean temperature in ROM_F can be indicative of the stronger SST variability. Comparing the correlation of vertical motion between ROM_P and ROM_F, the vertical velocity is correlated more deeply and strongly in ROM_F than ROM_P (Figs. 5b and d): in ROM_P, the significantly correlated vertical motion is limited to 40m while the vertical motion in ROM_F is significantly correlated down to 60-80m.

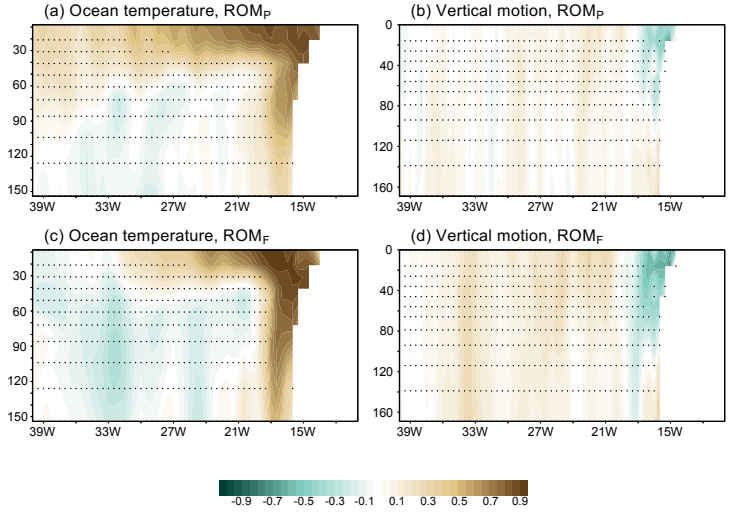

Figure 5: Vertical-longitudinal seciton of the correlation between the Dakar Index and (left) ocean temperature and (right) vertical motion averaged between 9°N and 14°N for (top) ROM_P and (bottom) ROM_F. The dots denote no significance of correlation.

Figures 6a-d show the composite of ocean temperature anomalies during Dakar Niño and Niñas in ROM_P and ROM_F, respectively. The definition of the Dakar Niño and Niña events is the detrended Dakar Index anomaly more and less respectively than + and - standard deviation of the Dakar Index. Similar to the correlation plot (Fig. 5), the temperature anomalies in ROM_P are large around 40m depth in both Niño and Niña and their magnitudes are almost identical (±1.8K, Figs. 6a and b). Interestingly, the temperature anomalies in ROM_F around 40 m depth are more pronounced during the Dakar Niñas

https://doi.org/10.5194/egusphere-2023-2494
Preprint. Discussion started: 1 December 2023

than Niños (Figs. 6c and d). In addition, the temperature anomaly associated with the Dakar Niñas penetrates more deeply in ROM_F than in ROM_P (Figs. 6b and d). That is, the amplification of the variability under global warming is mainly induced by the Dakar Niñas in our simulation. The surface to subsurface ocean is heated up following climate change, but its vertical distribution is heterogeneous (Fig.6e). The ocean surface experiences more efficient warming than the sub-surface. The
205 difference in warming is particularly large around 40m and upper levels where the temperature anomalies due to Dakar Niño/Niña variability and its change is the most intense (Fig. 6a-d). In addition to the vertical motion change, this reinforced stratification at 40m depth can be implicative for the strengthened Dakar Niño/Niña variability.

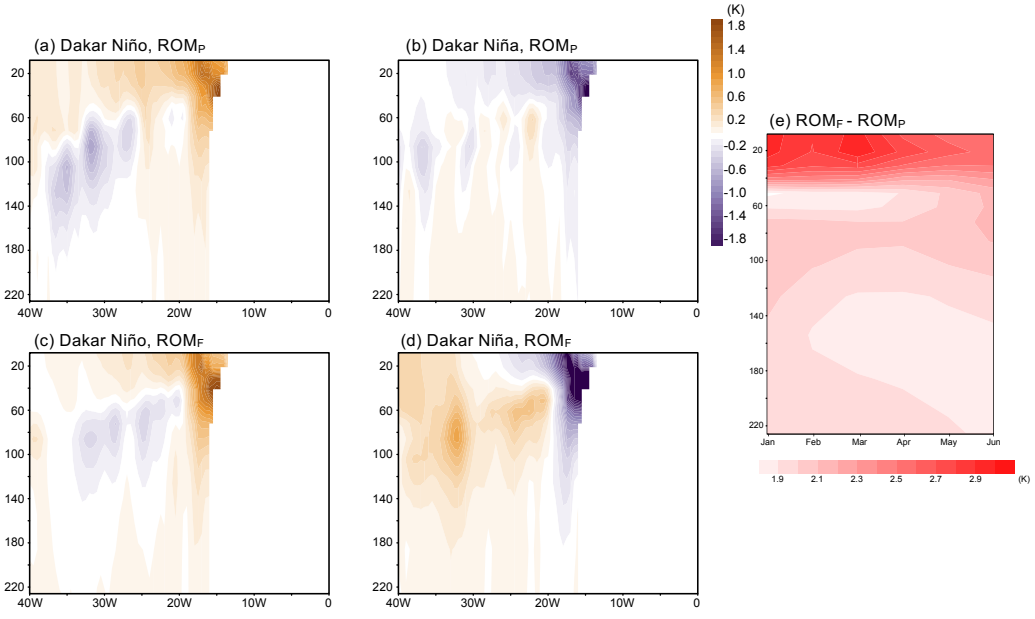

210 **Figure 6:** (a)-(d) Composite vertical-longitudal seciton of the temperature anomalies (K) for Dakar Niño/Niña in ROM_P and ROM_F in March. (e) Vertical-temporal section of the monthly climatological ocean temperature difference between ROM_F and ROM_P averaged over 9°N-14°N and 20°W-16°W.

4. Discussion and Summary

215 ### 4.1 Why is the Dakar Niño/Niña variability amplified?

The simulations of the high-resolution regionally coupled model, ROM have shown that the Dakar Niño/Niña variability in March will be reinforced under global warming, especially for the Dakar Niñas. According to Oettli et al. (2016), the Dakar Niño is driven mainly by changes in alongshore local surface wind and the surface wind changes are investigated in more details here.

220 The standard deviation of meridional wind stress anomalies is given in Fig. 7. In the observation, the high variability associated with the Azores high-pressure system (e.g., Davis et al., 1997) is found between 24°N and 30°N (Fig. 7a). Apart

https://doi.org/10.5194/egusphere-2023-2494
Preprint. Discussion started: 1 December 2023

from that, the meridional wind variability is relatively strong along the northwestern African coast down to 9°N as well. ROM_P, basically, is able to capture the spartial pattern of meridional wind variability: the coastal largest variability locates around 20°N (Fig. 7b) while the variability around 12°N and 20°W is somewhat overestimated resulting in forming two cores of high variability (in the observation, the second core around 12°N is much smaller and it is located more offshore as shown in Fig. 7a). Under global warming (Fig. 7c), the coastal wind variability is reinforced while the positions of the two cores are not changed. Inversely, the meridional wind variability over the open ocean between 24°N and 30°N does not seem to change as much as the coastal region (Figs. 7b and c) indicating that the wind variability might be more relevant due to local effects.

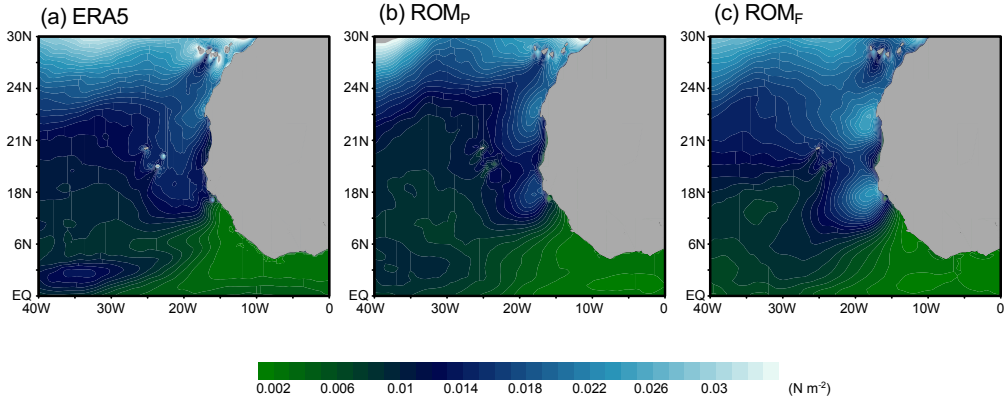

Figure 7: Standard deviation of the meridional wind stress in March for (a) ERA5, (b) ROM_P, and (c) ROM_F.

A possible explanation for the localized change in the surface wind is the land-sea heat contrast proposed by Bakun (1990). According to Bakun (1990), in the context of global warming, terrestrial regions will heat up faster and intensely than oceanic region, which will increase the land-sea heat contrast and consequently strengthen the equatorward coastal low-level jet and corresponding upwelling. Figure 8 shows the composite anomalies of 2m temperature during Dakar Niños and Dakar Niñas in ERA5 and ROM simulations. In the ERA5, the 2m temperature anomalies show a land-sea thermal contrast, but the 2m temperature anomalies over the land (signs are opposite to the Dakar Niños/Niñas near the coast) are located far from the western African coast (around 0° to 20°E, Figs. 8a and b). ROM_P can reproduce the terrestrial 2m temperature anomalies realistically in the case of Dakar Niño and Niña although its amplitude is weaker than that in ERA5 (Figs. 8c and d).

Conversely, the land-sea thermal contrast associated with the 2m temperature anomalies is more pronounced in ROM_F (Figs. 8c fand f). During the Dakar Niño events, the magnitude of cool anomaly over the continent is almost identical in both present and future climate, but spatially, land-surface temperature anomaly shifts more westward and the zonal surface temperature gradient can be weakened around the coastal region, especially, around 9°N-12°N (Fig. 8b). In the case of the Dakar Niñas, the land surface temperature anomaly shifts more westward similarly to the case of the Dakar Niñas and

https://doi.org/10.5194/egusphere-2023-2494
Preprint. Discussion started: 1 December 2023

additionally, its amplitude is much larger in ROM_F than in ROM_P (Figs. 8c and d). This situation can strengthen the zonal thermal contrast and the alongshore (upwelling-favorable) wind can be more effectively generated. In climatology, the ROM simulations show that the desert amplification (e.g., Cook and Vizy, 2015; Zhou, 2016) is pronounced in the western Africa under RCP8.5 scenario (not shown).

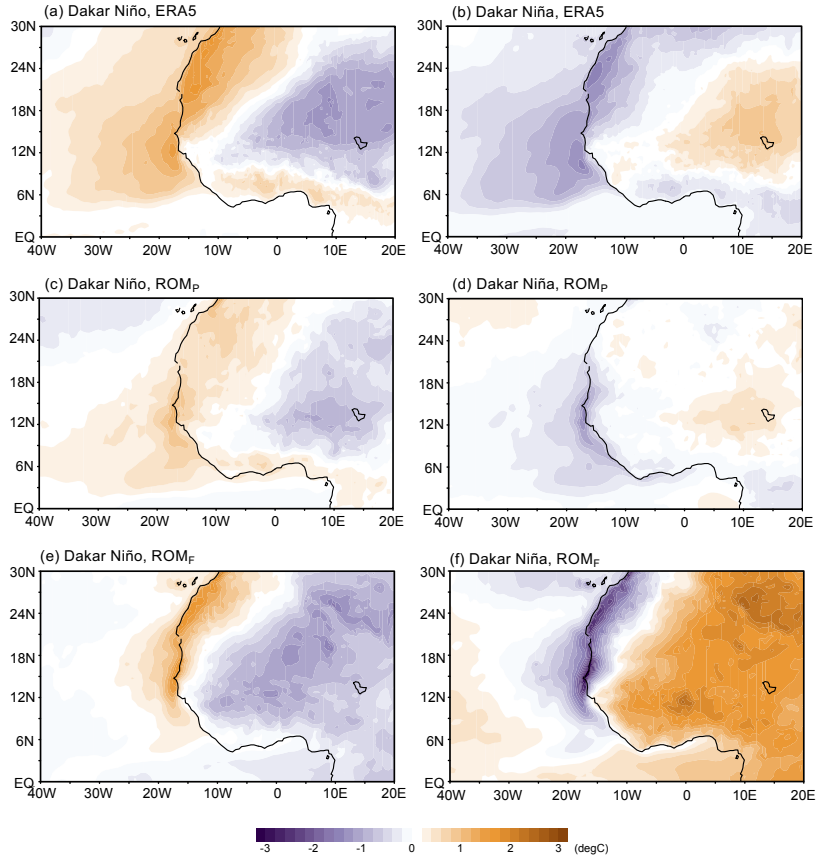

Figure 8: Composite anomalies of the 2m temperature averaged during (left) Dakar Niño/ /(right) Niña events in (top)ERA5, (middle) ROM_p , and (bottom) ROM_F in March.

This land-sea thermal contrast anomalies can be also indicated by sea level pressure (SLP) anomalies (Fig.9). In ERA5, the SLP anomalies shows a dipole pattern roughly over the Atlantic Ocean and the continent (Figs. 9a and b). While the SLP anomaly over the Atlantic can be relevant to the Azores high pressure, the SLP anomalies over the Sahara connect to the SLP anomalies over the Mediterranean and the SLP anomaly over the continent appears to be more responsible for creating the SLP zonal gradient along the coast, in particular, case of Dakar Niña (Fig. 2b). The ROM_P can represent this

https://doi.org/10.5194/egusphere-2023-2494
Preprint. Discussion started: 1 December 2023

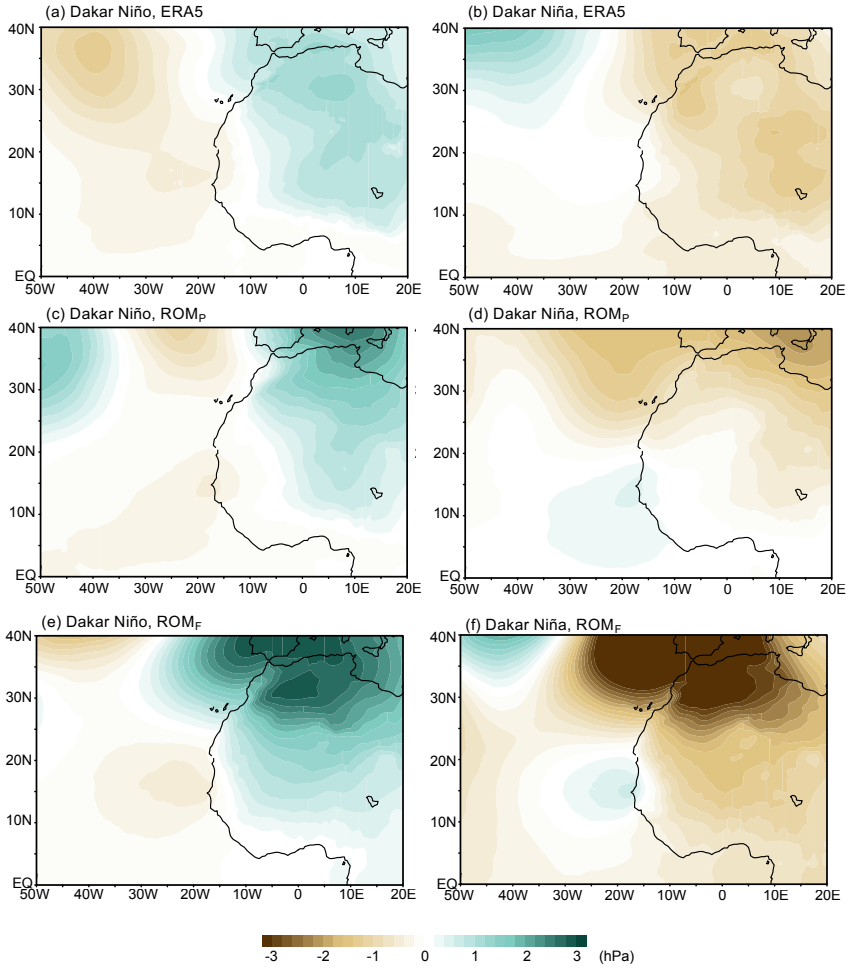

Figure 9: Same as Fig. 8 , but for sea level pressure in a wider domain.

SLP anomaly pattern that connects to the Mediterranean although the Azores high anomalies are not as clear as ERA5 (Figs. 9c and d). However, the cores of the continental SLP anomalies are located around 0 to 20°E, which is in line with ERA5. In the ROM_F, the continental SLP anomalies intensify as the 2m temperature anomalies are strengthened (Figs. 8e, f, 9e and f). Interestingly, the Mediterranean SLP anomalies are intensively reinforced in both cases and accordingly the Sahara SLP anomalies are stronger creating a sharper zonal SLP gradient along the western Africa coast. It is reported that the inter-annual variability in the temperature experiences future intensification in the Mediterranean region under global warming (Giorgi and Lionello, 2008) and the Mediterranean SLP anomalies are also expected to be amplified in the future.

4.2 Conclusion and future works

https://doi.org/10.5194/egusphere-2023-2494
Preprint. Discussion started: 1 December 2023

This study has investigated the future change of Dakar Niño variability in March employing a high-resolution regionally-coupled model, ROM with comparison between 1980-2010 and 2066-2099 under the highest emission scenario. Our model simulations show the intensification of Dakar Niño variability, especially Dakar Niña (cool SST anomaly) events. Stronger variability of SST can be explained by the stronger local alongshore wind variability inducing a deeper connection between the surface and subsurface and stronger vertical velocity variability. The alongshore wind variability can be enhanced by the well-developed thermal contrast anomaly around the west African coast based on the statement of Bakun (1990). Moreover, we found that the corresponding Saharan sea level pressure (SLP) anomalies are extended from the Mediterranean region and the Mediterranean SLP is reinforced intensively.

In addition, the stronger stratification at 40m depth might also cause the reinforcement of the Dakar Niño/Niña variability. This stronger stratification can be also due to the vertically-heterogeneous warming between the surface and subsurface (e.g., Vazquez et al., 2023).

Our discussion and argument are based on local-/regional-scale changes of surface wind and land-sea thermal/surface pressure contrast. However, as the previous studies suggest, the tropical Pacific inter-annual variability like El Niños tends to initialize the north tropical Atlantic variability including Dakar Niños via atmospheric bridge (e.g., Lopez-Parages et al., 2020; Oettli et al., 2016), we will need to consider such teleconnection and its future change. In addition, over the north Atlantic, other dominant climate mode like North Atlantic Oscillation (NAO, e.g., Hurrell et al., 2001) plays a crucial role in climate and weather variability over the Euro-Mediterranean region modulating the Azores high-pressure system (e.g., Brandimarte et al., 2011; Lopez-Moreno et al., 2011). Therefore, it will be desired to explore the linkages between Dakar Niño and other climate modes under global warming.

Code Availability

The codes used in this study can be accessed at Zonode repository, 10.5281/zenodo.10244333.

Data Availability

The data used in this study can be accessed at Zonode repository, 10.5281/zenodo.10244333.

Author Contributions

SK, VR, and WC contributed to conceptualizing the study and had discussions on the results. SK mainly performed the analyses. DSV and WC have demonstrated all the simulations used in this study. CG and MLB contributed to improving interpretation of the results and discussion. All co-authors contributed to drafting the manuscript and revising it.

Competing Interests

All co-authors declare that there is no conflict and competing interests.

https://doi.org/10.5194/egusphere-2023-2494
Preprint. Discussion started: 1 December 2023

Acknowledgement

SK was supported by EU Horizon 2020 TRIATLAS project (agreement number: 817578) and Giner de los Ríos 2021/22 program by University of Alcalá. RV was supported through a doctoral grant at University of Ferrara and University of Cadíz, the Spanish Ministry of Science, Innovation and Universities (I+D+I PID2021-128656OB-100) and the Plan Propio UCA 2022-23. WC and CG were funded by the Alcalá University project (PIUAH21/CC-058) and the Spanish Ministry of Science, Innovation and Universities, through grant (I+D+I PID2021-128656OB-100). DVS was supported by the Germany-Sino Joint Project (ACE, No. 2019YFE0125000 and 01LP2004A) and MHESRF scientific task № FMWE-2024-0028. MLB has received funding from the European Union's Horizon 2020 Research and Innovation Program for the project BENGUP under the Marie Skłodowska-Curie grant agreement ID 101025655. The simulations were performed at the German Climate Computing Center (DKRZ), granted by its Scientific Steering Committee (WLA) under project ID ba0987. All authors would like to express their gratefulness to Prof. Noel S. Keenlyside at the University of Bergen/BCCR for his constructive comments and discussions on this work.

References

Aristegui, J., Barton, E. D., Alvarez-Salgado, X. A., Santos, A. M. P., Figueiras, F. G., Kifani, S., Hernandez-Leon, S., Mason, E., Machu, E., and Demarcq, H.: Sub-regional ecosystem variability in the Canary Current upwelling. *Progress in Oceanography*, *83*(1-4), 33-48. https://doi.org/10.1016/j.pocean.2009.07.031, 2009

Arrasate-Lopez, M., Tuset, V. M., Santana, J. I., Garcia-Mederos, A., Ayza, O., and Gonzalez, J. A.: Fishing methods for sustainable shrimp fisheries in the Canary Islands (North-West Africa). *African Journal of Marine Science*, *34*(3), 331-339.https://doi.org/10.2989/1814232x.2012.725281 , 2012.

Bachelery, M. L., Illig, S., and Rouault, M.: Interannual Coastal Trapped Waves in the Angola-Benguela Upwelling System and Benguela Nino and Nina events. *Journal of Marine Systems*, *203*. https://doi.org/ARTN 103262,10.1016/j.jmarsys.2019.103262 , 2020

Bakun, A.: Global Climate Change and Intensification of Coastal Ocean Upwelling. *Science*, *247*(4939), 198-201. https://doi.org/DOI 10.1126/science.247.4939.198, 1990.

Barton, E. D., Aristegui, J., Tett, P., Canton, M., Garcia-Braun, J., Hernandez-Leon, S., Nykjaer, L., Almeida, C., Almunia, J., Ballesteros, S., Basterretxea, G., Escanez, J., Garcia-Weill, L., Hernandez-Guerra, A., Lopez-Laatzen, F., Molina, R., Montero, M. F., Navarro-Perez, E., Rodriguez, J. M., . . . Wild, K.: The transition zone of the Canary Current upwelling region. *Progress in Oceanography*, *41*(4), 455-504. https://doi.org/Doi 10.1016/S0079-6611(98)00023-8 , 1998.

Becognee, P., Almeida, C., Barrera, A., Hernandez-Guerra, A., and Hernandez-Leon, S.: Annual cycle of clupeiform larvae around Gran Canaria Island, Canary Islands. *Fisheries Oceanography*, *15*(4), 293-300. https://doi.org/10.1111/j.1365-2419.2005.00390.x , 2006.

Block, K., and Mauritsen, T.: Forcing and feedback in the MPI-ESM-LR coupled model under abruptly quadrupled CO2. *Journal of Advances in Modeling Earth Systems*, *5*(4), 676-691. https://doi.org/10.1002/jame.20041 , 2013.

Bracegirdle, T. J., Holmes, C. R., Hosking, J. S., Marshall, G. J., Osman, M., Patterson, M., and Rackow, T.: Improvements in Circumpolar Southern Hemisphere Extratropical Atmospheric Circulation in CMIP6 Compared to CMIP5. *Earth and Space Science*, *7*(6). https://doi.org/UNSP e2019EA001065, 10.1029/2019EA001065 , 2020.

https://doi.org/10.5194/egusphere-2023-2494
Preprint. Discussion started: 1 December 2023

Brandimarte, L., Di Baldassarre, G., Bruni, G., D'Odorico, P., and Montanari, A.: Relation Between the North-Atlantic Oscillation and Hydroclimatic Conditions in Mediterranean Areas. *Water Resources Management*, *25*(5), 1269-1279. https://doi.org/10.1007/s11269-010-9742-5 , 2011.

Cabos, W., de la Vara, A., Alvarez-Garcia, F. J., Sanchez, E., Sieck, K., Perez-Sanz, J. I., Limareva, N., and Sein, D. V.: Impact of ocean-atmosphere coupling on regional climate: the Iberian Peninsula case. *Climate Dynamics*, *54*(9-10), 4441-4467. https://doi.org/10.1007/s00382-020-05238-x , 2020.

Cabos, W., Sein, D. V., Pinto, J. G., Fink, A. H., Koldunov, N. V., Alvarez, F., Izquierdo, A., Keenlyside, N., and Jacob, D.: The South Atlantic Anticyclone as a key player for the representation of the tropical Atlantic climate in coupled climate models. *Climate Dynamics*, *48*(11), 4051-4069. https://doi.org/10.1007/s00382-016-3319-9 , 2017

Choudhury, B. A., Rajesh, P. V., Zahan, Y., and Goswami, B. N.: Evolution of the Indian summer monsoon rainfall simulations from CMIP3 to CMIP6 models. *Climate Dynamics*, *58*(9-10), 2637-2662. https://doi.org/10.1007/s00382-021-06023-0 , 2022.

Colberg, F., and Reason, C. J. C.: A model study of the Angola Benguela Frontal Zone: Sensitivity to atmospheric forcing. *Geophysical Research Letters*, *33*(19). https://doi.org/Artn L19608, 10.1029/2006gl027463 , 2006

Cook, K. H., and Vizy, E. K.: Detection and Analysis of an Amplified Warming of the Sahara Desert. *Journal of Climate*, *28*(16), 6560-6580. https://doi.org/10.1175/Jcli-D-14-00230.1 , 2015.

Counillon, F., Keenlyside, N. S., Wang, S., Devillers, M., Gupta, A., Koseki, S., and Shen, M.-L.: Framework for an ocean-connected supermodel of the Earth System. J*ournal of Advances in Modeling Earth System*, **15**, e2022MS003310, https://doi.org/10.1029/2022MS003310, 2023.

Crespo, L. R., Prigent, A., Keenlyside, N., Koseki, S., Svendsen, L., Richter, I., and Sanchez-Gomez, E.: Weakening of the Atlantic Nino variability under global warming. *Nature Climate Change*, *12*(9), 822-+. https://doi.org/10.1038/s41558-022-01453-y , 2022.

Cropper, T. E., Hanna, E., and Bigg, G. R.: Spatial and temporal seasonal trends in coastal upwelling off Northwest Africa, 1981-2012. *Deep-Sea Research Part I-Oceanographic Research Papers*, *86*, 94-111. https://doi.org/10.1016/j.dsr.2014.01.007 , 2014.

Davis, R. E., Hayden, B. P., Gay, D. A., Phillips, W. L., and Jones, G. V.: The North Atlantic subtropical anticyclone. *Journal of Climate*, *10*(4), 728-744. https://doi.org/Doi 10.1175/1520-0442(1997)010<0728:Tnasa>2.0.Co;2 ,1997.

de la Vara, A., Cabos, W., Sein, D. V., Sidorenko, D., Koldunov, N. I. V., Koseki, S., Soares, P. M. M., and Danilov, S.: On the impact of atmospheric vs oceanic resolutions on the representation of the sea surface temperature in the South Eastern Tropical Atlantic. *Climate Dynamics*, *54*(11-12), 4733-4757. https://doi.org/10.1007/s00382-020-05256-9 , 2020.

Dee, D. P., Uppala, S. M., Simmons, A. J., Berrisford, P., Poli, P., Kobayashi, S., Andrae, U., Balmaseda, M. A., Balsamo, G., Bauer, P., Bechtold, P., Beljaars, A. C. M., van de Berg, L., Bidlot, J., Bormann, N., Delsol, C., Dragani, R., Fuentes, M., Geer, A. J., . . . Vitart, F.: The ERA-Interim reanalysis: configuration and performance of the data assimilation system. *Quarterly Journal of the Royal Meteorological Society*, *137*(656), 553-597. https://doi.org/10.1002/qj.828 , 2011.

Deppenmeier, A. L., Haarsma, R. J., LeSager, P., and Hazeleger, W.: The effect of vertical ocean mixing on the tropical Atlantic in a coupled global climate model. *Climate Dynamics*, *54*(11-12), 5089-5109. https://doi.org/10.1007/s00382-020-05270-x , 2020.

Dippe, T., Greatbatch, R. J., and Ding, H.: On the relationship between Atlantic Nio variability and ocean dynamics. *Climate Dynamics*, *51*(1-2), 597-612. https://doi.org/10.1007/s00382-017-3943-z , 2018.

Eyring, V., Bony, S., Meehl, G. A., Senior, C. A., Stevens, B., Stouffer, R. J., and Taylor, K. E.: Overview of the Coupled Model Intercomparison Project Phase 6 (CMIP6) experimental design and organization. *Geoscientific Model Development*, *9*(5), 1937-1958. https://doi.org/10.5194/gmd-9-1937-2016 , 2016.

Giorgetta, M. A., Jungclaus, J., Reick, C. H., Legutke, S., Bader, J., Bottinger, M., Brovkin, V., Crueger, T., Esch, M., Fieg, K., Glushak, K., Gayler, V., Haak, H., Hollweg, H. D., Ilyina, T., Kinne, S., Kornblueh, L., Matei, D., Mauritsen, T., . . . Stevens, B.: Climate and carbon cycle changes from 1850 to 2100 in MPI-ESM simulations for the Coupled Model Intercomparison Project phase 5. *Journal of Advances in Modeling Earth Systems*, *5*(3), 572-597. https://doi.org/10.1002/jame.20038 , 2013.

https://doi.org/10.5194/egusphere-2023-2494
Preprint. Discussion started: 1 December 2023

Giorgi, F., and Lionello, P.: Climate change projections for the Mediterranean region. *Global and Planetary Change*, *63*(2-3), 90-104. https://doi.org/10.1016/j.gloplacha.2007.09.005 , 2008.

Gomez-Letona, M., Ramos, A. G., Coca, J., and Aristegui, J.: Trends in Primary Production in the Canary Current Upwelling System-A Regional Perspective Comparing Remote Sensing Models. *Frontiers in Marine Science*, *4*. https://doi.org/ARTN 370, 10.3389/fmars.2017.00370, 2017.

Good, S. A., Embury, O., Bulgin, C. E., and Mittaz, J.: ESA Sea Surface Temperature Climate Change Initiative (SST_cci): Level 4 Analysis Climate Data Record, version 2.0. https://doi.org/10.5285/aced40d7cb964f23a0fd3e85772f2d48 , 2019.

Haarsma, R. J., Roberts, M. J., Vidale, P. L., Senior, C. A., Bellucci, A., Bao, Q., Chang, P., Corti, S., Fuckar, N. S., Guemas, V., von Hardenberg, J., Hazeleger, W., Kodama, C., Koenigk, T., Leung, L. R., Lu, J., Luo, J. J., Mao, J. F., Mizielinski, M. S., . . . von Storch, J. S.: High Resolution Model Intercomparison Project (HighResMIP v1.0) for CMIP6. *Geoscientific Model Development*, *9*(11), 4185-4208. https://doi.org/10.5194/gmd-9-4185-2016 , 2016.

Hersbach, H., Bell, B., Berrisford, P., Hirahara, S., Horanyi, A., Munoz-Sabater, J., Nicolas, J., Peubey, C., Radu, R., Schepers, D., Simmons, A., Soci, C., Abdalla, S., Abellan, X., Balsamo, G., Bechtold, P., Biavati, G., Bidlot, J., Bonavita, M., . . . Thepaut, J. N.: The ERA5 global reanalysis. *Quarterly Journal of the Royal Meteorological Society*, *146*(730), 1999-2049. https://doi.org/10.1002/qj.3803 , 2020.

Hurrell, J. W., Kushnir, Y., and Visbeck, M.: Climate - The North Atlantic oscillation. *Science*, *291*(5504), 603-605. https://doi.org/DOI 10.1126/science.1058761 , 2001.

Jacob, D.: A note to the simulation of the annual and inter-annual variability of the water budget over the Baltic Sea drainage basin. *Meteorology and Atmospheric Physics*, *77*(1-4), 61-73. https://doi.org/DOI 10.1007/s007030170017 , 2001.

Jungclaus, J. H., Fischer, N., Haak, H., Lohmann, K., Marotzke, J., Matei, D., Mikolajewicz, U., Notz, D., and von Storch, J. S.: Characteristics of the ocean simulations in the Max Planck Institute Ocean Model (MPIOM) the ocean component of the MPI-Earth system model. *Journal of Advances in Modeling Earth Systems*, *5*(2), 422-446. https://doi.org/10.1002/jame.20023 , 2013.

Koseki, S., Giordani, H., and Goubanova, K.: Frontogenesis of the Angola-Benguela Frontal Zone. *Ocean Science*, *15*(1), 83-96. https://doi.org/10.5194/os-15-83-2019 , 2019.

Koseki, S., and Koungue, R. A. I.: Regional atmospheric response to the Benguela Ninas. *International Journal of Climatology*, *41*, E1483-E1497. https://doi.org/10.1002/joc.6782 , 2021.

Koseki, S., Vazquez, R., Cabos, W., Gutierrez, C., Sein, D. M., and Bacherery, M.-L., 2023. ROM data and code for Dakar Niño variability under global warming investigated by a high-resolution regionally coupled model. 10.5281/zenodo.10244333, 2023

Koungue, R. A. I., Brandt, P., Luebbecke, J., Prigent, A., Martins, M. S., and Rodrigues, R. R.: The 2019 Benguela Nino. *Frontiers in Marine Science*, *8*. https://doi.org/ARTN 800103, 10.3389/fmars.2021.800103 , 2021.

Koungue, R. A. I., Rouault, M., Illig, S., Brandt, P., and Jouanno, J.: Benguela Ninos and Benguela Ninas in Forced Ocean Simulation From 1958 to 2015. *Journal of Geophysical Research-Oceans*, *124*(8), 5923-5951. https://doi.org/10.1029/2019jc015013 , 2019.

Lazaro, C., Fernandes, M. J., Santos, A. M. P., and Oliveira, P.: Seasonal and interannual variability of surface circulation in the Cape Verde region from 8 years of merged T/P and ERS-2 altimeter data. *Remote Sensing of Environment*, *98*(1), 45-62. https://doi.org/10.1016/j.rse.2005.06.005 , 2005.

Lopez-Moreno, J. I., Vicente-Serrano, S. M., Moran-Tejeda, E., Lorenzo-Lacruz, J., Kenawy, A., and Beniston, M.: Effects of the North Atlantic Oscillation (NAO) on combined temperature and precipitation winter modes in the Mediterranean mountains: Observed relationships and projections for the 21st century. *Global and Planetary Change*, *77*(1-2), 62-76. https://doi.org/10.1016/j.gloplacha.2011.03.003 , 2011.

Lopez-Parages, J., Auger, P. A., Rodriguez-Fonseca, B., Keenlyside, N., Gaetan, C., Rubino, A., Arisido, M. W., and Brochier, T.: El Nino as a predictor of round sardinella distribution along the northwest African coast. *Progress in Oceanography*, *186*. https://doi.org/ARTN 102341, 10.1016/j.pocean.2020.102341 , 2020.

Marsland, S. J., Haak, H., Jungclaus, J. H., Latif, M., and Roske, F.: The Max-Planck-Institute global ocean/sea ice model with orthogonal curvilinear coordinates. *Ocean Modelling*, *5*(2), 91-127. https://doi.org/Pii S1463-5003(02)00015-X, Doi 10.1016/S1463-5003(02)00015-X , 2003,

https://doi.org/10.5194/egusphere-2023-2494
Preprint. Discussion started: 1 December 2023

Martin-Rey, M., and Lazar, A.: Is the boreal spring tropical Atlantic variability a precursor of the Equatorial Mode? *Climate Dynamics*, *53*(3-4), 2339-2353. https://doi.org/10.1007/s00382-019-04851-9 , 2019.

Mittelstaedt, E.: The Ocean Boundary Along the Northwest African Coast - Circulation and Oceanographic Properties at the Sea-Surface. *Progress in Oceanography*, *26*(4), 307-355. https://doi.org/Doi 10.1016/0079-6611(91)90011-A , 1991.

Ndoye, S., Capet, X., Estrade, P., Sow, B., Dagorne, D., Lazar, A., Gaye, A., and Brehmer, P.: SST patterns and dynamics of the southern Senegal-Gambia upwelling center. *Journal of Geophysical Research-Oceans*, *119*(12), 8315-8335. https://doi.org/10.1002/2014jc010242 , 2014.

Oettli, P., Morioka, Y., and Yamagata, T.: A Regional Climate Mode Discovered in the North Atlantic: Dakar Nino/Nina. *Scientific Reports*, *6*. https://doi.org/ARTN 18782, 10.1038/srep18782 , 2016.

Pardo, P. C., Padin, X. A., Gilcoto, M., Farina-Busto, L., and Perez, F. F.: Evolution of upwelling systems coupled to the long-term variability in sea surface temperature and Ekman transport. *Climate Research*, *48*(2-3), 231-246. https://doi.org/10.3354/cr00989 , 2011.

Pastor, M. V., Pelegri, J. L., Hernandez-Guerra, A., Font, J., Salat, J., and Emellanov, M.: Water and nutrient fluxes off Northwest Africa. *Continental Shelf Research*, *28*(7), 915-936. https://doi.org/10.1016/j.csr.2008.01.011 , 2008.

Perez-Hernandez, M. D., Hernandez-Guerra, A., Fraile-Nuez, E., Comas-Rodriguez, I., Benitez-Barrios, V. M., Dominguez-Yanes, J. F., Velez-Belchi, P., and De Armas, D.: The source of the Canary current in fall 2009. *Journal of Geophysical Research-Oceans*, *118*(6), 2874-2891. https://doi.org/10.1002/jgrc.20227 , 2013.

Priestley, M. D. K., Ackerley, D., Catto, J. L., Hodges, K. I., McDonald, R. E., and Lee, R. W.: An Overview of the Extratropical Storm Tracks in CMIP6 Historical Simulations. *Journal of Climate*, *33*(15), 6315-6343. https://doi.org/10.1175/Jcli-D-19-0928.1 , 2020.

Richter, I., and Tokinaga, H.: An overview of the performance of CMIP6 models in the tropical Atlantic: mean state, variability, and remote impacts. *Climate Dynamics*, *55*(9-10), 2579-2601. https://doi.org/10.1007/s00382-020-05409-w , 2020.

Richter, I., and Xie, S. P.: On the origin of equatorial Atlantic biases in coupled general circulation models. *Climate Dynamics*, *31*(5), 587-598. https://doi.org/10.1007/s00382-008-0364-z , 2008.

Rouault, M., Illig, S., Lubbecke, J., and Koungue, R. A. I.: Origin, development and demise of the 2010-2011 Benguela Nino. *Journal of Marine Systems*, *188*, 39-48. https://doi.org/10.1016/j.jmarsys.2017.07.007 , 2018.

Santana-Falcon, Y., Mason, E., and Aristegui, J.: Offshore transport of organic carbon by upwelling filaments in the Canary Current System. *Progress in Oceanography*, *186*. https://doi.org/ARTN 102322, 10.1016/j.pocean.2020.102322 , 2020.

Schevenhoven, F., Keenlyside, N., Counillon, F., Carrassi, A., Chapman, W. E., Devilliers, M., Gupta, A., Koseki, S., Selten, F., Shen, M.-L., Wang, S., Weiss, J. B., Wiegerinch, W., and Duane, G. S.: Supermodeling: Improving Predictions with an Ensemble of Interacting Models. *Bulletin of the American Meteorological Society*. **104**(9), E1670-E1686, https://doi.org/10.1175/BAMS-D-22-0070.1 , 2023.

Sein, D. V., Groger, M., Cabos, W., Alvarez-Garcia, F. J., Hagemann, S., Pinto, J. G., Izquierdo, A., de la Vara, A., Koldunov, N. V., Dvornikov, A. Y., Limareva, N., Alekseeva, E., Martinez-Lopez, B., and Jacob, D.: Regionally Coupled Atmosphere-Ocean-Marine Biogeochemistry Model ROM: 2. Studying the Climate Change Signal in the North Atlantic and Europe. *Journal of Advances in Modeling Earth Systems*, *12*(8). https://doi.org/ARTN e2019MS001646, 10.1029/2019MS001646 , 2020.

Sein, D. V., Mikolajewicz, U., Groger, M., Fast, I., Cabos, W., Pinto, J. G., Hagemann, S., Semmler, T., Izquierdo, A., and Jacob, D.: Regionally coupled atmosphere-ocean-sea ice-marine biogeochemistry model ROM: 1. Description and validation. *Journal of Advances in Modeling Earth Systems*, *7*(1), 268-304. https://doi.org/10.1002/2014ms000357 , 2015.

Shen, M. L., Keenlyside, N., Selten, F., Wiegerinck, W., and Duane, G. S.: Dynamically combining climate models to "supermodel" the tropical Pacific. *Geophysical Research Letters*, *43*(1), 359-366. https://doi.org/10.1002/2015gl066562 , 2016.

https://doi.org/10.5194/egusphere-2023-2494
Preprint. Discussion started: 1 December 2023

Soares, P. M. M., Lima, D. C. A., Semedo, A., Cardoso, R. M., Cabos, W., and Sein, D.: The North African coastal low level wind jet: a high resolution view (vol 53, pg 1211, 2019). *Climate Dynamics*, *53*(1-2), 1231-1231. https://doi.org/10.1007/s00382-018-4475-x , 2019.

Sylla, A., Mignot, J., Capet, X., and Gaye, A. T.: Weakening of the Senegalo-Mauritanian upwelling system under climate change. *Climate Dynamics*, *53*(7-8), 4447-4473. https://doi.org/10.1007/s00382-019-04797-y , 2019.

Toniazzo, T., and Koseki, S.: A Methodology for Anomaly Coupling in Climate Simulation. *Journal of Advances in Modeling Earth Systems*, *10*(8), 2061-2079. https://doi.org/10.1029/2018ms001288 , 2018.

Vazquez, R., Parras-Berrocal, I., Cabos, W., Sein, D. V., Mananes, R., and Izquierdo, A.: Assessment of the Canary current upwelling system in a regionally coupled climate model. *Climate Dynamics*, *58*(1-2), 69-85. https://doi.org/10.1007/s00382-021-05890-x , 2022.

Vazquez, R., Parras-Berrocal, I., Koseki, S., Cabos, W., Sein, D. V., Izquierdo, A.: Seasonality of coastal upwelling trends in the Mauritania-Senegalese region under RCP8.5 climate change scenarios. *Science of The Total Environment*. *898*, 166391, https://doi.org/10.1016/j.scitotenv.2023166391, 2023.

Voldoire, A., Exarchou, E., Sanchez-Gomez, E., Demissie, T., Deppenmeier, A. L., Frauen, C., Goubanova, K., Hazeleger, W., Keenlyside, N., Koseki, S., Prodhomme, C., Shonk, J., Toniazzo, T., and Traore, A. K.: Role of wind stress in driving SST biases in the Tropical Atlantic. *Climate Dynamics*, *53*(5-6), 3481-3504. https://doi.org/10.1007/s00382-019-04717-0 , 2019.

Yang, Y., Wu, L. X., Cai, W. J., Jia, F., Ng, B., Wang, G. J., and Geng, T.: Suppressed Atlantic Nino/Nina variability under greenhouse warming. *Nature Climate Change*, *12*(9), 814-+. https://doi.org/10.1038/s41558-022-01444-z , 2022.

Zhou, L. M.: Desert Amplification in a Warming Climate. *Scientific Reports*, *6*. https://doi.org/ARTN 31065, 10.1038/srep31065 , 2016.

Zuo, H., Balmaseda, M. A., Tietsche, S., Mogensen, K., and Mayer, M.: The ECMWF operational ensemble reanalysis-analysis system for ocean and sea ice: a description of the system and assessment. *Ocean Science*, *15*(3), 779-808. https://doi.org/10.5194/os-15-779-2019 , 2019.